Supporting Information

Aluminum doped Sodium manganese hexa cyano ferrate cathode for high-rate safe Na-ion battery

P Mohana Sundaram[a,b], S.K.Vineeth[c,d], Soumyashree Das[e], C. Sanjaykumar[a,f], P Sennu [b], Chhail Bihari Soni[a], Mahesh Chandra[a], Sungjemmenla[a], Hemant Kumar[e], Vipin Kumar*[a,c]

[a] *Department of Energy Science and Engineering, Indian Institute of Technology, Delhi, Hauz Khas, New Delhi 110016, India*

[b] *Indian Oil Corporation Limited, R&D Centre, Faridabad 121007, India*

[c] *University of Queensland- IIT Delhi Academy of Research (UQIDAR), Indian Institute of Technology Delhi, Hauz Khas, New Delhi, India 110016*

[d] *Australian Institute for Bioengineering and Nanotechnology (AIBN), The University of Queensland, Brisbane, QLD 4072, Australia*

[e] *School of Basic Sciences, Indian Institute of Technology, Bhubaneswar*

[f] *School of Interdisciplinary Research (SIRe), Indian Institute of Technology, Delhi*

Corresponding E-mail: vkumar@dese.iitd.ac.in

Experimental section

S1-Synthesis of Sodium manganese hexa cyano ferrate

The cathode material (reference) sodium manganese hexa cyano ferrate was synthesized through a co-precipitation reaction[1] .0.96 g of $MnSO_4.H_2O$ and 1.67 g of trisodium citrate were dissolved in 100 ml of de-ionized Water (Solution A), and 3.36 g of sodium ferro cyanide deca hydrate [$Na_4Fe(CN)_6.10H_2O$] was dissolved in 100 ml of de-ionized Water (Solution B). Then, Solution A and B were fed with the flow rate of 1 ml per minute into Solution C, which contains 60 g Sodium nitrate ($NaNO_3$) dissolved in 200 ml of de-ionized water under stirring conditions at 25°C. The stirrer speed was maintained at 500 rpm. After 12 hours, the solution was taken out and subjected to vacuum filtration. After filtration, the white precipitate was collected and washed with water and ethanol five times. Then, the filtrate was collected and dried in a vacuum oven and maintained at a temperature of 120 ºC for 24 hours. After 24 hours, the dried sample was collected and subjected to further characterization.

S2-Synthesis of Aluminum doped sodium manganese hexacyano ferrate

0.96 g of $MnSO_4.H_2O$,3.15 g of Aluminum sulfate hexadeca hydrate $[Al_2(SO4)_3.16H_2O]$, and 1.67 g of tri-sodium citrate was dissolved in 100 ml of de-ionized Water (Solution A) and 3.36 g of Sodium ferrocyanide deca hydrate $[Na_4Fe(CN)_6.10H_2O]$ was dissolved in 100 ml of de-ionized Water (Solution B). Then, Solution A and B were fed with the flow rate of 1 ml per minute into Solution C, which contains 60 g Sodium nitrate ($NaNO_3$) dissolved in 200 ml of de-ionized water under stirring conditions at 25°C. The stirrer speed was maintained at 500 rpm. After 12 hours, the solution was removed and subjected to vacuum filtration. After filtration, the grey color precipitate was collected and washed with water and ethanol five times. After washing, the filtrate was collected and dried in a vacuum oven and maintained at 120 ºC for 24 hours. After 24 hours, the dried sample was collected and subjected to further characterization. A similar procedure was followed for various Aluminum sulfate concentrations (0.025 M to 0.2 M) and kept other reactant concentrations to study the effect of Aluminum doping in sodium manganese hexa cyano ferrate.

S3 Carbon coating on Sodium titanium phosphate

Sodium titanium phosphate has several advantages, such as higher sodium ion conductivity and better structural stability[2]. However, its use as a negative active material is limited due to its low electrical conductivity. The carbon coating can be provided on electrode material[3] to improve the electrical conductivity. Further, carbon coating may stabilize the SEI formation by restraining sodium ions from reacting with electrolytes[4]. The carbon coating on sodium titanium phosphate(NEI Corporation) is prepared from glucose as a carbon feed precursor[5]. In a typical synthesis procedure, 0.5g of carbon black,0.05 g of D-glucose, and 0.005 g of sodium ligno sulfonate (organic surfactant) were weighed and mixed. It was fed into 15 ml of de-ionized water and stirred for 15 minutes. After stirring, the mixture was subjected to sonication for 15 minutes, then 1 g of sodium titanium phosphate was fed into it. The resultant mixture was further sonicated for 15 minutes. The solution was dried at 120 ºC for 24 hours in a laboratory oven. The sample was collected and subjected to carbonization in the tubular furnace at 800 ºC for 4 hours in N_2 atmosphere. The as-obtained black material was used as an anode directly without further purification steps. The carbon content of carbon coated sodium titanium phosphate was analyzed by TGA (Figure S11).

S4-Analytical Characterizations

The structures of sodium manganese hexacyano ferrate (NMHCF) and Aluminum-doped sodium manganese hexacyano ferrate (Al-NMHCF) were measured by X-ray diffraction (Make: Panalytical, Model: Empyrean). The morphology was examined with a field emission scanning electron microscope (SEM: JEOL, Model: JSM6610LV) and a Transmission electron microscope (TEM, Make: JEOL, Model: JEM 2100). The oxidation states of elements are measured by using the XPS (ULVAC PHI). The metal contents of Al-doped sodium manganese hexacyano ferrate were evaluated by using an inductively coupled plasma-optical emission spectrometer (ICP-OES, Make: Thermo Scientific, Model: iCAP PRO XP Duo)

S4.1

The comparative of XPS spectra for pristine (Figure S6a, S6b) and Al-NMHCF (Figure S6c, S6d) are also provided. From Figure S6a and S6c both pristine and Al-NMHCF, the two peaks observed at ~642 eV, correspond to $Mn^{II}2p_{3/2}$ and $Mn^{III}2p_{3/2}$ respectively, Further, two peaks at 708 eV and 721 eV which correspond to $Fe^{II}2p_{3/2}$ and $Fe^{II}2p_{1/2}$ however peak intensity varies. Further, the ratio of Mn^{II}/Mn^{III} for Al-NMHCF is 1.29, and pristine NMHCF is 1.23.

S5-Preparation of the electrodes and electrochemical analysis of the cell

The cathode was prepared using 80 wt. % NMHCF or Al-NMHCF, 10 wt. % super p (carbon), and 10 wt. % polyvinylidene fluoride (PVDF). The anode was prepared using 80 wt. % carbon-coated sodium titanium phosphate, 10 wt. % super p (carbon) and 10 wt. % polyvinylidene fluoride. The mass loading of cathode active material was maintained at $1mg/cm^2$. 100 microliters of 35 M NaFSIwere used as a water-in-salt electrolyte (WIS), and a Whatman glass fiber was used as the separator. The cyclic voltammetry (CV) was measured by the electrochemical workstation (Biologic SAS, VSP-300). The charge/discharge tests were conducted on a battery tester (Biologic Science Instruments, BCS805).

S6-Water in Salt Electrolyte (WIS)

35 M NaFSI water in salt electrolyte prepared by 7.105 g sodium (I) bis (fluoro sulfonyl) imide-99.9% (procured from M/s Solvionic) dissolved in 1 ml of de-ionized water.

S6.1- Zinc Metal Foil

Zinc metal foil is selected vs Na foil due to water-in-salt electrolyte system and as sodium metal reacts with water very vigorously and produces hydrogen with an uncontrollable exothermic reaction, we refrained from employing Na metal. Considering safety aspects, Zn foil was selected instead of sodium metal foil as an anode for half-cell evaluation for the WIS electrolyte system.

S7- Galvanostatic Intermittent Titration (GITT)

The GITT test was conducted in full-cell with 0.39 mA current (corresponding to the current density of 200 mAg^{-1}) to charge the electrode up to 2.5 V and then discharged with 0.39 mA discharging current (corresponding to the current density of 200 mAg^{-1}). The duration of the current pulse was kept at 30 seconds, and the rest time was kept at 60 seconds[6].

The diffusion coefficient was calculated using equation (1)

$$D= (4/\pi\tau)\ [(m_B V_M)/(M_B A)]^2 [\Delta E_s/\Delta E_t] \quad \ldots\ldots..(1)$$

Where τ is the duration of the current pulse in sec, M_B (g $mol^{-1)}$ is the molecular weight of the electrode material, V_M is the molar volume, m_B is the weight of the active material in grams and A is the electrode surface area. ΔE_s denote the change in the steady-state voltage at a plateau and ΔE_t is the total change in cell voltage during pulse time

S7.1- Electrochemical Impedance Spectroscopy (EIS)

A lower SEI resistance suggests a stable and conductive SEI layer, which is crucial for protecting the electrode and ensuring long-term battery performance.[7] Furthermore, the charge transfer resistance reflects the ease of charge transfer across the electrode-electrolyte interface.

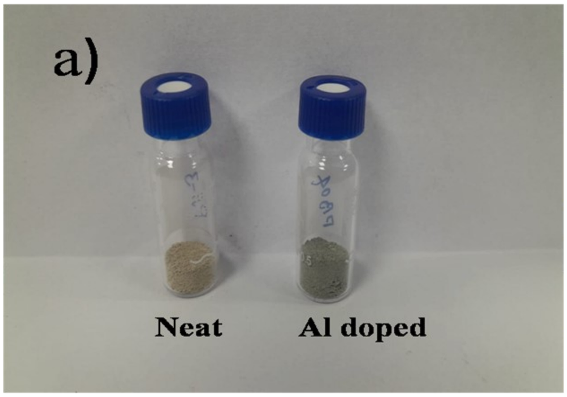

Figure S1 Images of Sodium manganese hexa cyano ferrate (Colorless) and Al-doped sodium manganese hexa cyano ferrate (Greenish grey color)

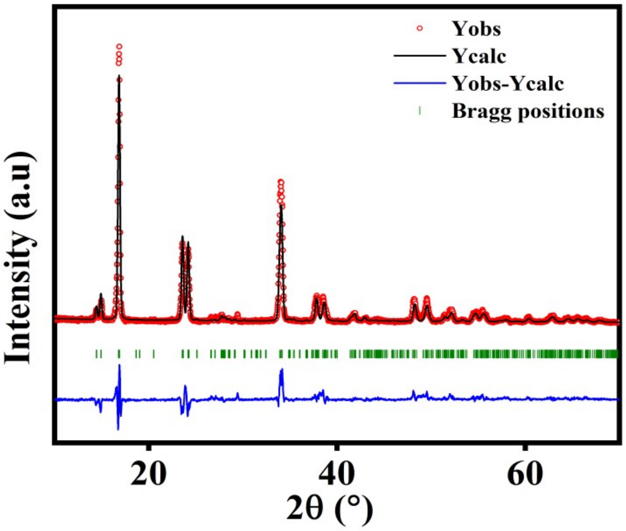

Figure S2 Rietveld refinement fittings of monoclinic phase of pristine NMHCF (Chi2: 4.61, Rp: 31.6 Rwp: 32.3 Rexp: 15.04, P21/n space group, monoclinic, a= 10.573237, b= 7.529434, c =7.342745Å & α =90 °, β= 91.96, γ =90 °)

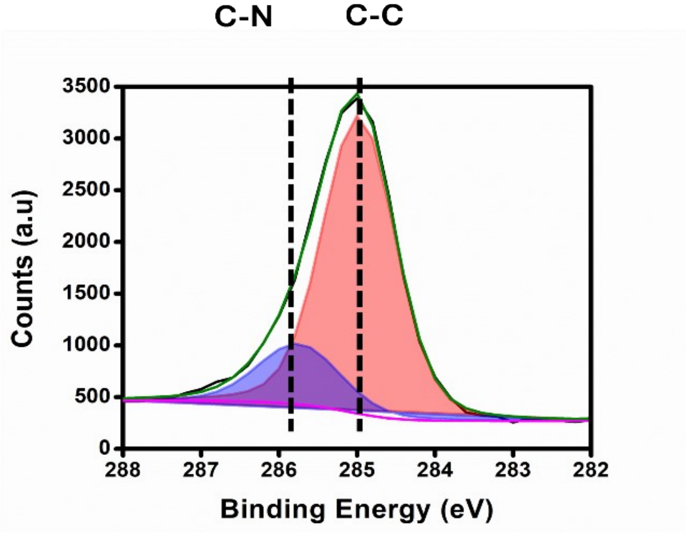

Figure S3 XPS peaks position of C-N and C-C

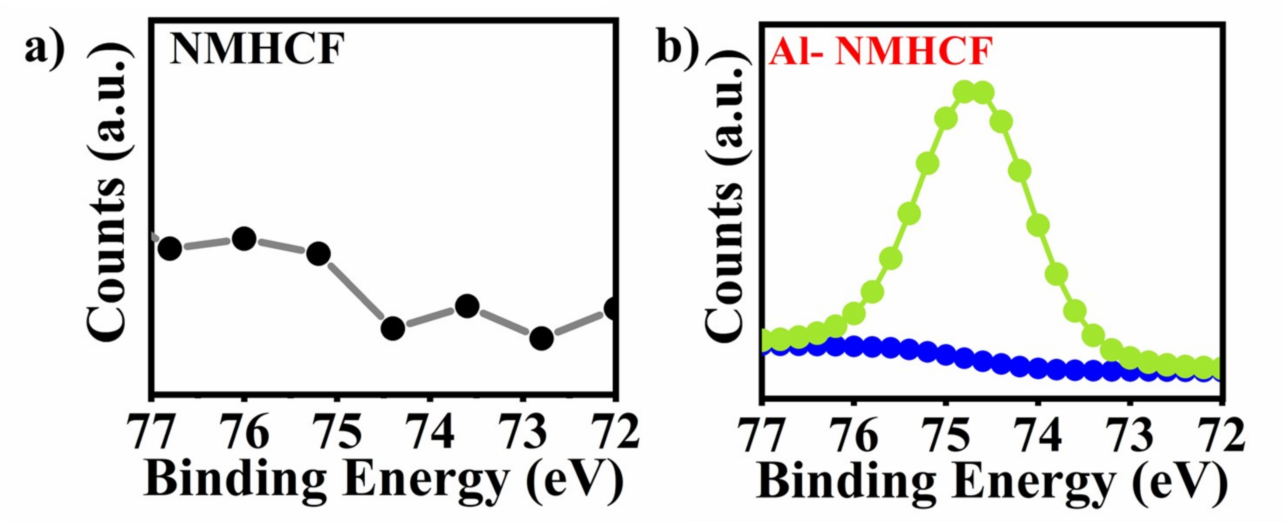

Figure S4 a) XPS nil Al peak position in NMHCF b) XPS Al peak position in Al-NMHCF

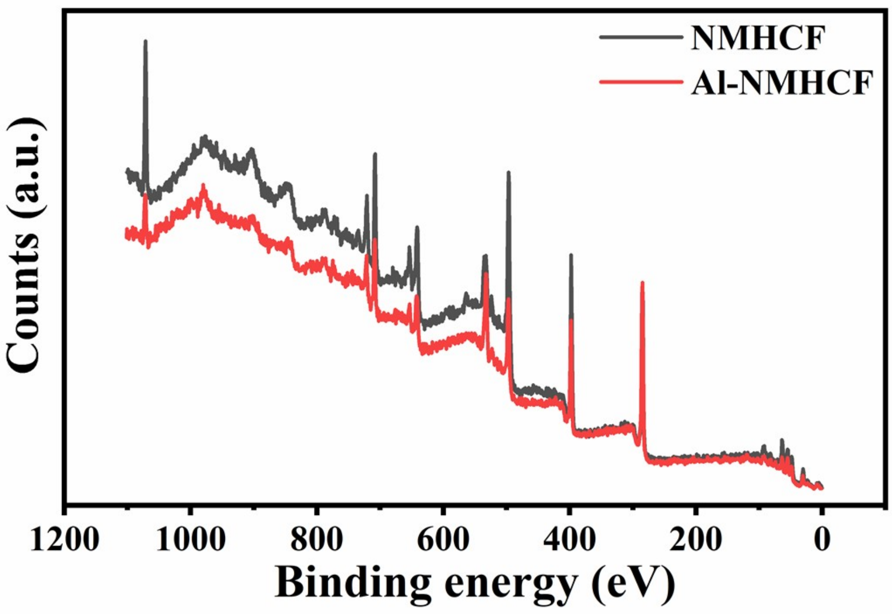

Figure S5 The survey XPS spectra of Pristine and Al-NMHCF

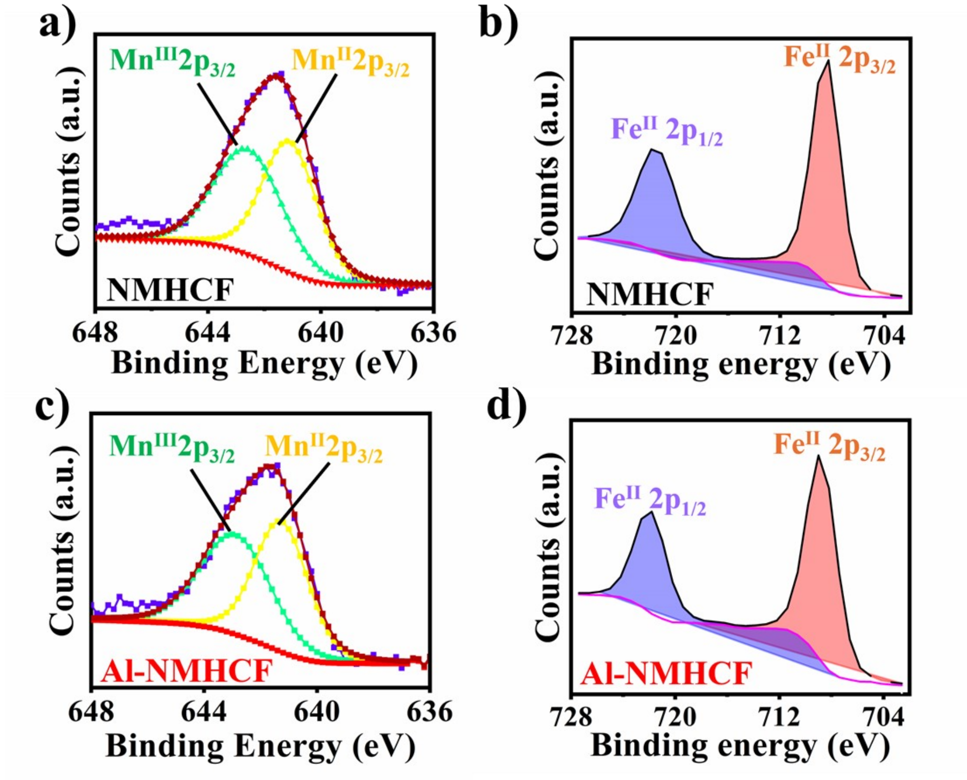

Figure S6 a) XPS Mn peaks of Pristine NMHCF b) XPS Fe peaks of pristine NMHCF c) XPS Mn peaks of Al-NMHCF d) XPS Fe peaks of Al-NMHCF

Table S1 Comparison of Surface Area and Pore size characteristics of NMHCF Vs Al-NMHCF

S. No	Property	NMHCF	Al-NMHCF
1	Surface area (m^2g^{-1})	4.28	9.76
2	Pore volume (cm^3g^{-1})	0.05	0.07
3	Average pore diameter (A°)	498.71	286.19

Table S2 Metal content analysis by ICP-OES for Aluminum doped sodium manganese hexa cyano ferrate

S. No	**Aluminium Sulphate concentration (M)**		**Metal content in sodium manganese hexacyanoferrate**			
		Metal content(m)	**Mass (%)**	**m/Al ratio**	**m/Na ratio**	**Mn/Fe Atomic ratio**
1	0.025	Fe	13.44	192	1.47	1.07
		Mn	14.19	202.71	1.55	
		Na	9.12	130.28		
		Al	0.07		0.0007	
2	0.05	Fe	12.46	17.8	1.16	0.94
		Mn	11.57	16.52	1.07	
		Na	10.72	15.31		
		Al	0.7		0.07	
3	0.1	Fe	13.42	11	1.84	1.004
		Mn	13.26	10.86	1.81	
		Na	7.29	5.97		
		Al	1.22		0.16	
4	0.2	Fe	5.70	0.81	0.55	0.90
		Mn	5.10	0.72	0.49	
		Na	10.37	1.48		
		Al	7.0		0.67	

Table S3 Comparison of metal content of NMHCF Vs Al-NMHCF

S. No	Metal content (ICP-AES)	NMHCF (wt%)	Al-NMHCF (0.05M) (wt%)	Atomic mass ratio of NMHCF	Atomic mass ratio of Al-NMHCF	Atomic mass ratio of Mn/Fe in NMHCF	Atomic mass ratio of Mn/Fe in Al-NMHCF
1	Fe	12.3	12.46	0.220	0.223	1.0	0.94
2	Mn	12.1	11.57	0.220	0.21		
3	Na	11.9	10.72				
4	Al	---	0.7				

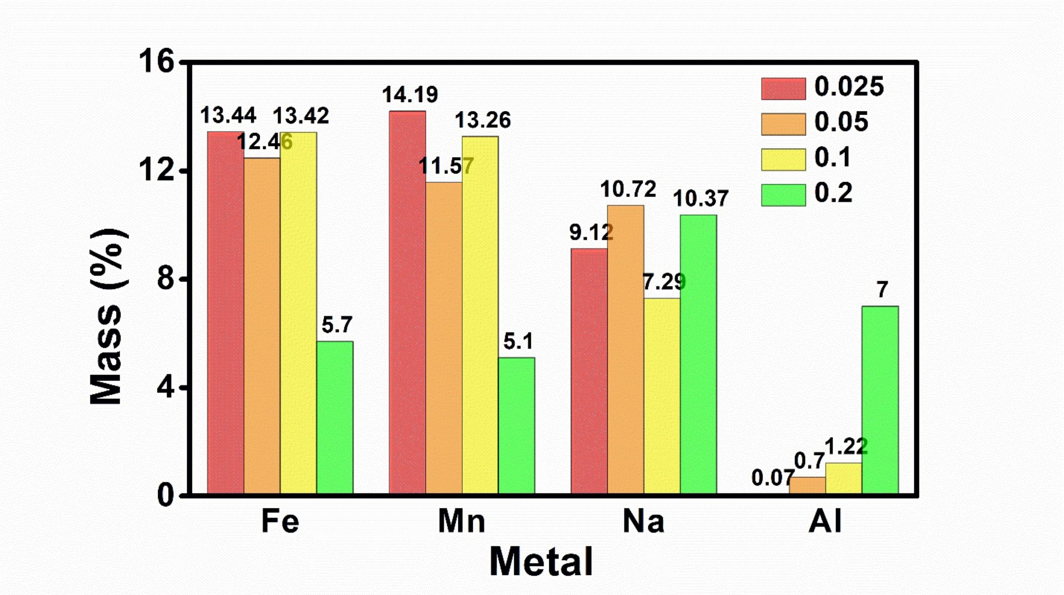

Figure S7 Metal content in various sodium manganese hexa cyano ferrate analysis by ICP-AES.

Table S4 Amount of water content in Al-doped NMHCF derived from 0.025M, 0.05M, 0.1M, and 0.2M Aluminium sulphate feed precursor

S. No	Aluminium sulphate concentration (M)	Total Water content (wt %) (TGA)
1	0.025	15
2	0.05	14
3	0.1	14.5
4	0.2	14

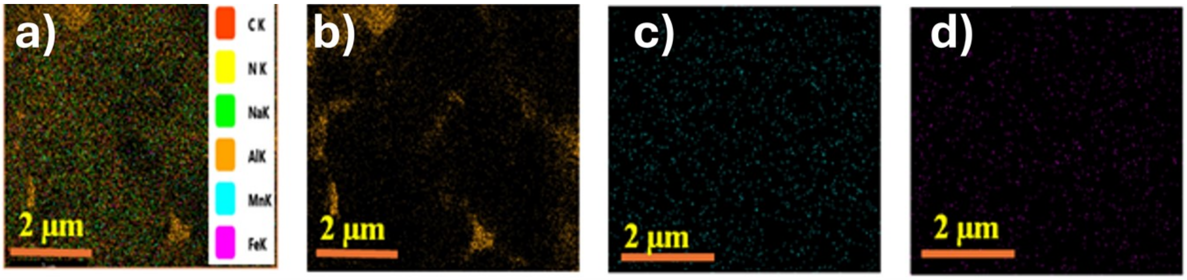

Figure S8 a) EDEX elemental map of Al-NMHCF b) EDEX-Al distribution in Al-NMHCF c) EDEX-Mn distribution in Al-NMHCF d) EDEX-Fe distribution

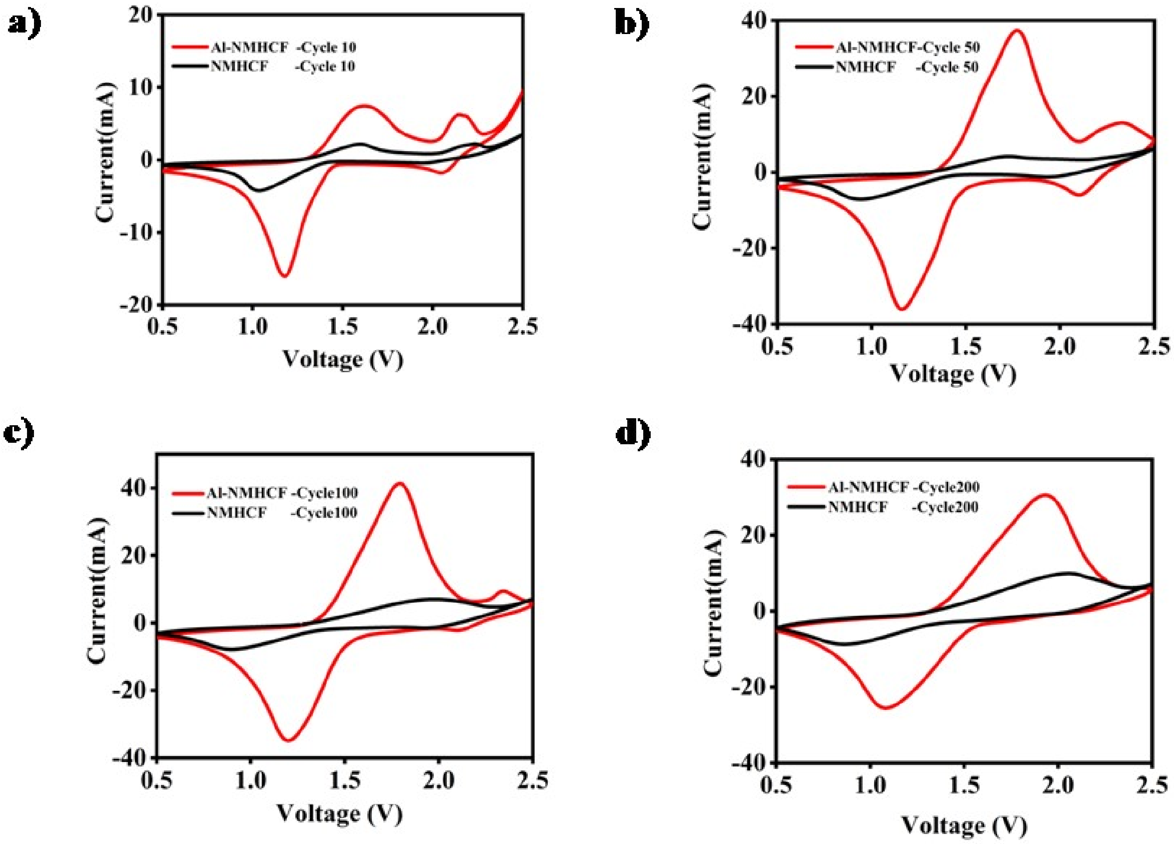

Figure S9 a) Half-cell CV comparison of pristine and Al-doped NMHCF (0.05M) at cycle 10 b) Half-cell CV comparison of pristine and Al-doped NMHCF (0.05M) at cycle 50 c) Half-cell CV comparison of pristine and Al-doped NMHCF (0.05M) at cycle 100, d) Half-cell CV comparison of pristine and Al-doped NMHCF (0.05M) at cycle 200

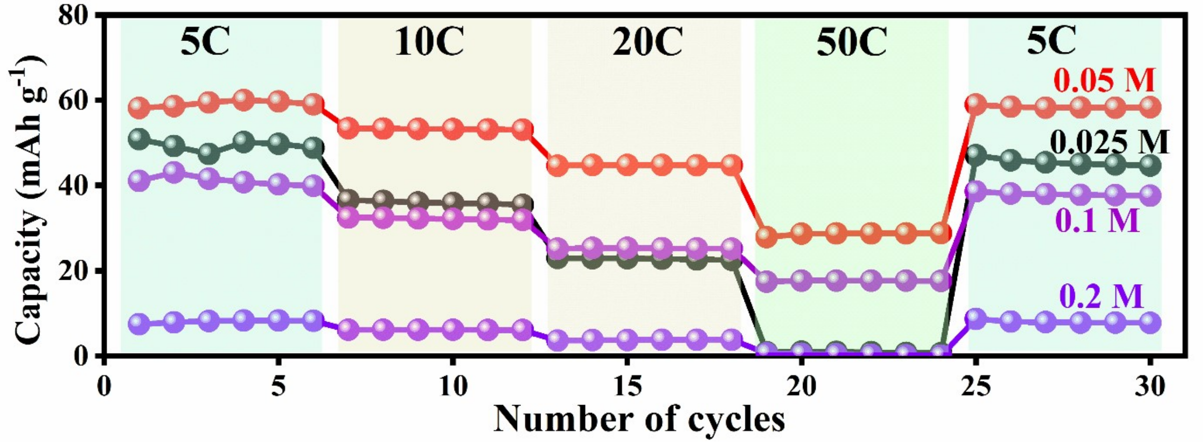

Figure S10 Half-cell high-rate performance diagram for Al-NMHCF synthesized through 0.025M,0.05M,0.1M and 0.2M $Al_2(SO4)_3$

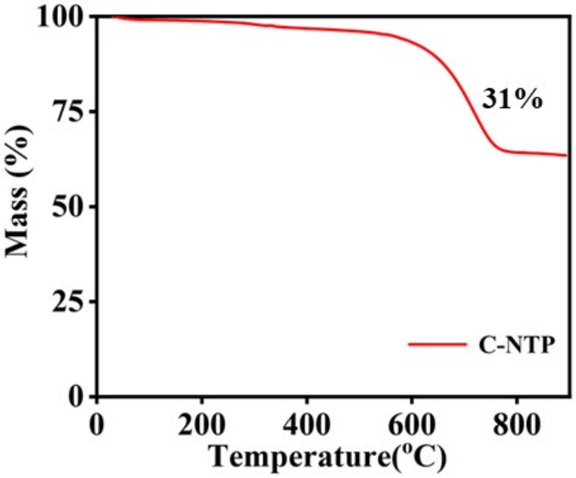

Figure S11 Thermal gravimetric analysis of C-NTP in Air

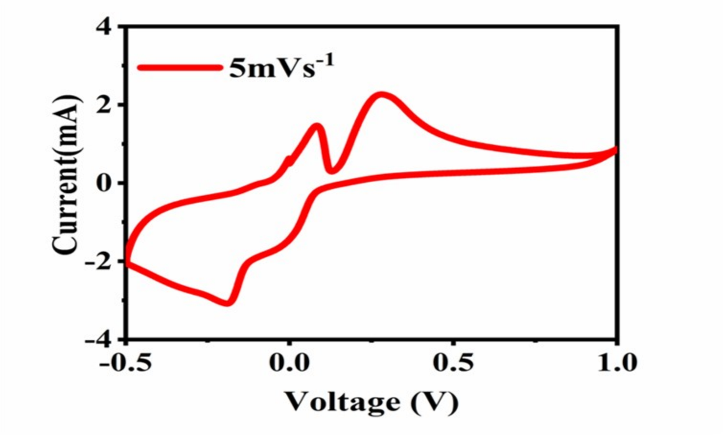

Figure S12 Half-cell CV of C-NTP at 5mVs^{-1}

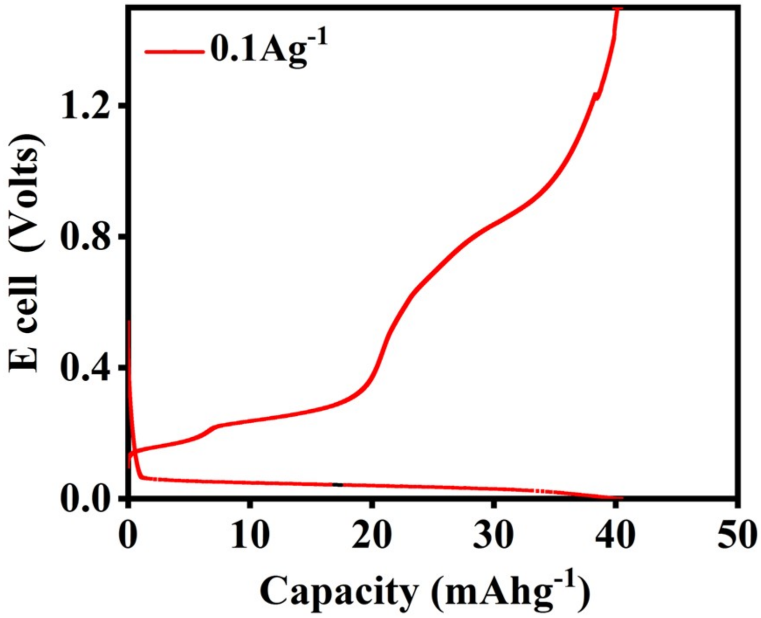

Figure S13 C-NTP capacity at 0.1Ag^{-1} in WIS (35 M NaFSI) electrolyte

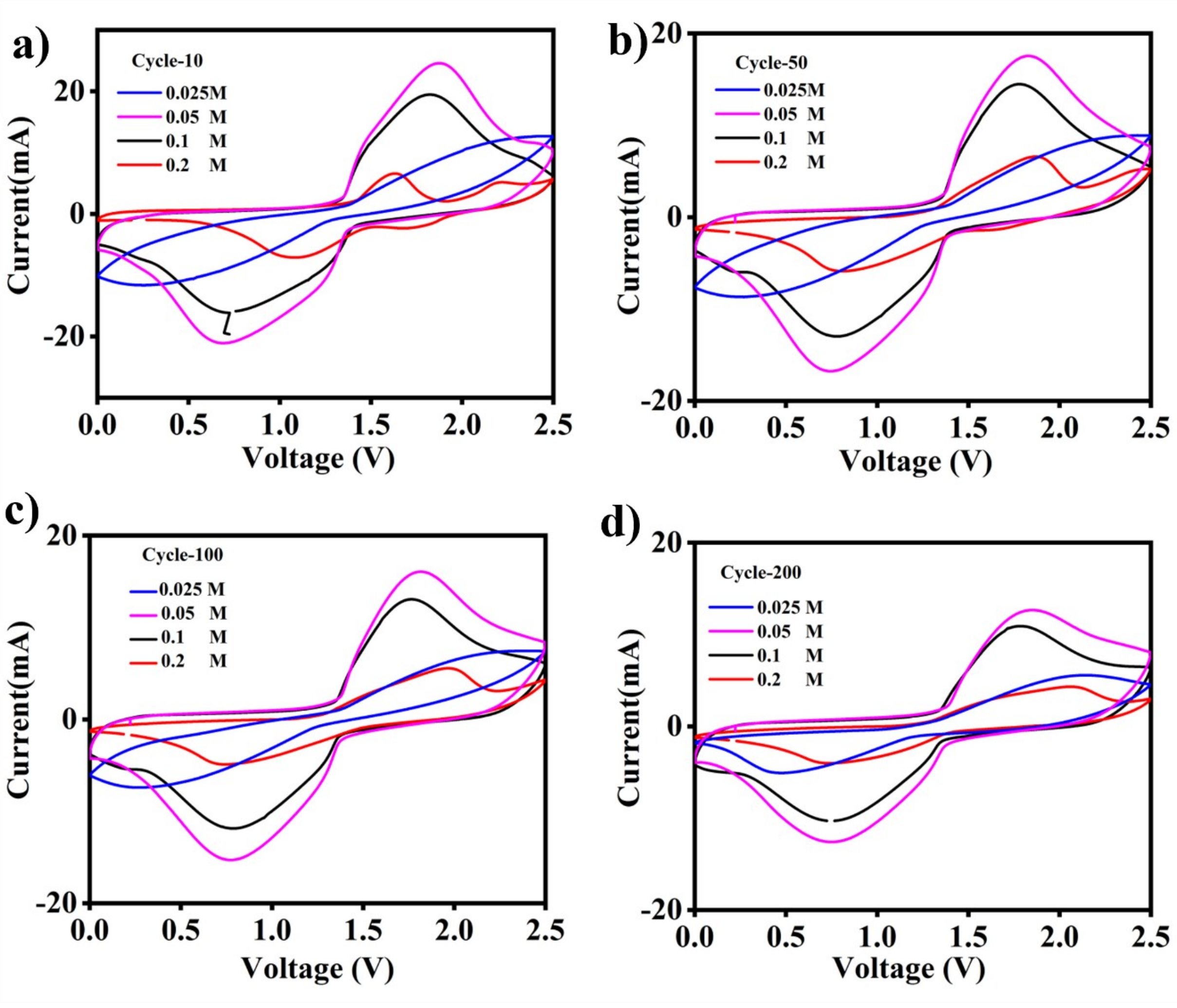

Figure S14 a) Full cell CV comparison of Al-doped NMHCF at various Aluminum sulphate feed precursor a) cycle 10 b) cycle 50 c) cycle 100 d) cycle 200

Table S5 Summary of electrochemical performance of NMHCF cathode materials in WIS and Organic electrolytes

Material	**WIS electrolyte**	**Organic electrolyte**	**Electrochemical performance**	**References**
NMHCF	1M $ZnSO_4$ (Aq)	---	53.3 $mAhg^{-1}$ (0.05Ag^{-1},120 Cycles)	[8]
NMHCF	17 M $NaClO_4$(WIS)	---	33 $mAhg^{-1}$ (0.2 Ag^{-1},100 cycles)	[9]
NMHCF	9M NaOTF + 22M TEAOTF	---	41 $mAhg^{-1}$ (0.1 Ag^{-1},200 cycles @ 90% capacity retention)	[10]
C-NMHCF	---	1M $NaPF_6$ +PC+10% FEC	120 $mAhg^{-1}$ (0.025 Ag^{-1})	[11]
Ni-NMHCF (Na1.76Ni0.04Mn0.96[Fe(CN)6]0.86□0.14·0.0005H2O)	---	1M $NaPF_6$+PC+2%FEC	140 $mAhg^{-1}$ @ 0.05 C	[12]
Ni-NMHCF	---	Organic	93 $mAhg^{-1}$	[13]
Al-NMHCF	35 M NaFSI (WIS)	---	64$mAhg^{-1}$ (0.1 Ag^{-1}), 53$mAhg^{-1}$ (0.8Ag^{-1},300 Cycles), 35$mAhg^{-1}$ (2Ag^{-1},300	Present Work

			Cycles), 17mAhg^{-1} (5Ag^{-1},300 Cycles)	

Table S6 Evaluation of capacity degradation at high rate charging and discharging

S. No	Charging and discharging current rate (Ag^{-1})	~ C-Rate	Capacity degradation rate (mAhg^{-1})
1	0.8	~8	0.12
2	2	~20	0.05
3	5	~50	0.05

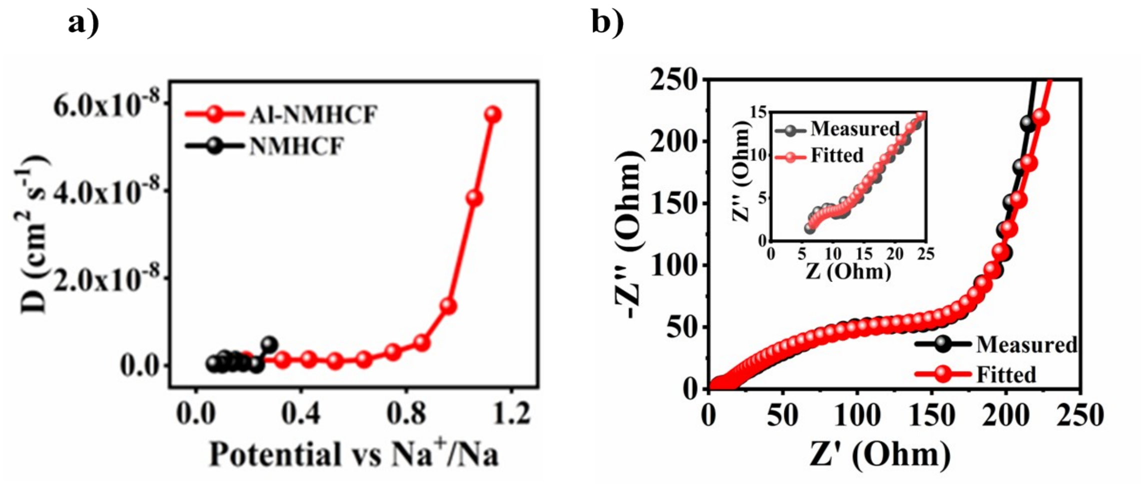

Figure S15 a) Comparative full cell GITT-diffusion coefficient evaluation for NMHCF Vs Al-NMHCF b) EIS evaluation of Al-NMHCF

S8-Postmortem analysis of the Al-NMHCF

Since NMHCF is subjected to the phase change upon charge and discharge leading to capacity fading the phase change in Al-doped NMHCF was examined before and after applying different potentials. The XRD analysis (**Figures 4a and 4b**) unveiled that the Al-doped NMHCF bears no phase change upon charging and discharging. Further, no peak shift is observed during charging, demonstrating no change in lattice parameters upon de-sodiation. This indicates that the Al-doped cubic structure is more stable. Al doping inhibits the phase change during cycling and maintains the cubic phase structure. To monitor the effect of cycling on the phase change of the Al-doped NMHCF, the cells were subjected to 300 cycles. The XRD remains intact, and no split peaks (monoclinic phase) are observed, indicating the absence of phase change upon cycling.

The cathode electrolyte inter-phase (CEI), which is largely debatable in Li-ion batteries, though less discussed, plays a critical role in Na-ion batteries. The possibility of the CEI formation was examined using XPS.

S9 -Computational Methods

DFT calculations were performed using the Vienna Ab Initio Package (VASP) with a plane-wave basis set and the projector-augmented wave method to account for core electrons. For all compounds, the atom position and lattice vectors were relaxed by using generalized gradient approximations (GGAs) parameterized by the Perdew-Burke-Ernzerhof (PBE) functional. The Hubbard-like correction (DFT+U) method was used with two effective U (Ueff) values for Fe ([Ar] 3d6 4s2: 4.3 eV) and Mn ([Ar] 3d5 4s2: 3.0 eV) to add the extra on-site interaction energies on the d-metal. For all structural optimizations and energy, the energy and forces converged to within 10-4 eV and 0.05 eV Å-1, respectively. Spin polarization was included in all cases. It has used a cubic centered 4 × 4 × 4 k-point grid and a plane-wave energy cutoff of 400 eV. The climbing image nudged elastic band (CI-NEB) method was employed to calculate the diffusion barriers for Na-ion migration.

To understand the origin of the stable cycle-life, DFT calculations were performed. DFT calculations were performed for different phases of sodium manganese hexacyanoferrate ($Na_xMnFe(CN)_6$) to examine the effect of Al doping on formation energy and volume expansion of its structures (**Figures 4d-k**). The formation energies of both phases are calculated to study the stability of Al-doped or pristine NMHCF. The formation energy of all $Na_xPFe(CN)_6$ intercalation compounds is defined with respect to their de-sodiated phases and the Na bodycentered cubic crystal as the reference state. The expression used for characterizing this formation energy, E_f, is as follows [14].

Ef = E (NaxPFe(CN)$_6$) - E (PFe(CN)$_6$) - xE (Na_bcc)

Where P indicates the transition metals and/or dopants, E (NaxPFe(CN)$_6$) is the energy of NaxPFe(CN)$_6$ compound per formula unit (fu), E (PFe(CN)$_6$) is the energy of PFe(CN)$_6$ per fu, and E (Na-bcc) is the per-atom energy of Na-bcc. The negative value of the formation energy indicates the thermodynamic stability of the intercalation compound against the separation into the most stable forms[15].

The optimized lattice constants for the cubic (C-MnFe(CN)$_6$) and monoclinic (M-MnFe(CN)$_6$) phases of MHCF are shown in **Table 1.** The calculated formation energy of the cubic phase of $Na_{0.55}Al_{0.09}MnFe(CN)_6$ is about -5.511 eV, which is much less than the formation energy (-2.168 eV) for the monoclinic phase of the un-doped $Na_{0.98}MnFe(CN)_6$. The formation energy studies imply that the Al-doped cubic phase of NMHCF is more stable than the pristine monoclinic phase. It is due to the selective stabilization effect of aluminum on different crystal structures, and it suggests that the cubic phase is highly stabilized as compared to the monoclinic phase. In the Al-doped NMHCF, the interaction between Na^+ and $N\boldsymbol{\delta}^-$ atoms is significantly reduced at the site of Al due to the ineffective Hubbard-like correction for the outermost p-orbital of the Al atom. As a result, the position of sodium ions is predicted to be shifted towards the FeC_6 sites. **Figures 4f-k** present the calculated structure of the un-doped and doped NMHCF. Different valance states are possible since Mn–N and Fe–C coordinate with different atoms, i.e., MnN6 and FeC_6.

During the charging and discharging process, there is a significant volume change to occur in the cathode active materials. The volume change directly affects the cyclic stability of the cathode. The substantial change in volume causes a collapse in crystal lattice leading to decreased cyclic stability. The rate of volume change (ΔV_x)at various Na concentrations for $Na_xPFe(CN)_6$ is calculated by equation

$$\Delta V_x = \frac{V_x - V_0}{V_0} \times 100\%$$ [16]

Where V_x and V_0 are the volumes of sodiated and de-sodiated unit cells of $Na_xPFe(CN)_6$.

The DFT analysis shows that the introduction of Al in NMHCF leads to cubic phase formation due to lower formation energy requirement as compared to pristine monoclinic NMHCF. Further, experimental results also affirm that Al doping leads to the formation of a cubic phase. The cubic phase Al-NMHCF is more stable than the monoclinic phase pristine NMHCF, which is also ensured by DFT analysis due to lower change in volume as compared to the monoclinic phase during sodiation and desodiation. The comparative analysis of previous work on WIS electrolytes with NMHCF and Al-NMHCF (present work) on electrochemical performance and cycle life is given in **Table S5**. Further, C-F and CF_2 peaks (**Figure S17**) at 289.3 eV, and 291.4 eV [17], were also observed respectively.

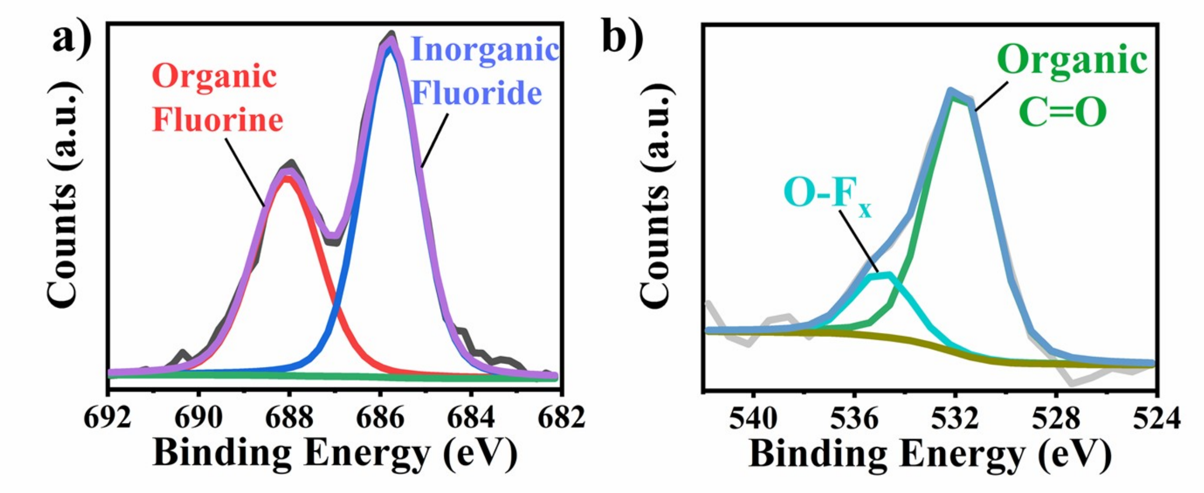

Figure S16 Post-cycling high-resolution XPS of a) F and b) O present in the Al-NHMCF

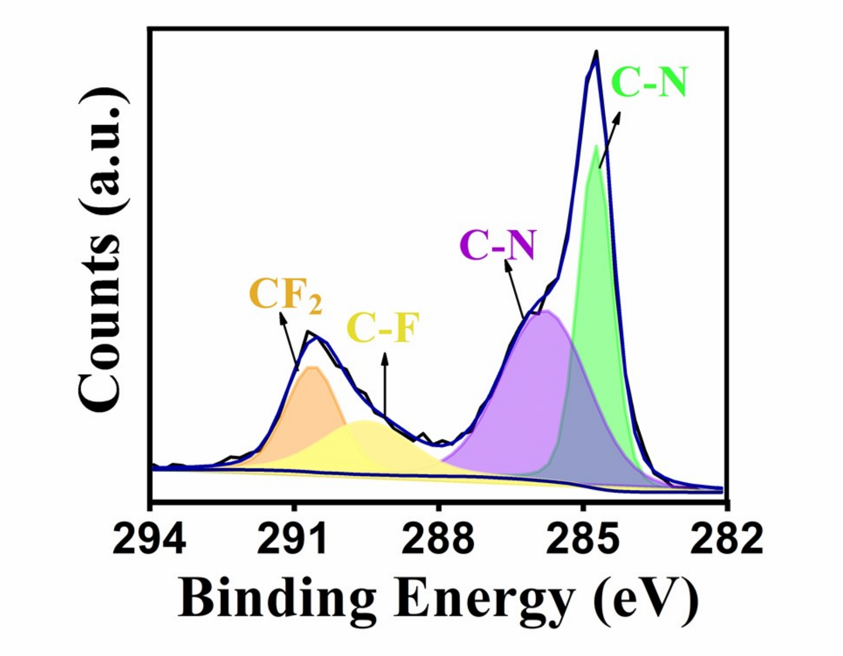

Figure S17 XPS peaks position of C-C, C-N, C-F and CF$_2$ after cycling

Table S7 Lattice parameters of different simulated structures

S. No	Structures	Lattice parameters
1	C-MnFe(CN)$_6$	a = b = c = 10.2293 Å, $\alpha = \beta = \gamma = 90°$, V = 1070.37 Å^3
2	M-MnFe(CN)$_6$	a = 10.3555 Å, b = 7.3695 Å, c = 7.1759 Å, $\alpha = \gamma = 90°$, $\beta = 92.114°$, V = 547.26 Å^3
3	C-Na$_{0.5}$Al$_{0.25}$Mn$_{0.75}$Fe(CN)$_6$	a = b = c = 10.3315 Å, $\alpha = \beta = \gamma = 90°$, V = 1102.77 Å^3
4	M-Na$_1$MnFe(CN)$_6$	a = 10.7434 Å, b = 7.6456 Å, c = 7.4448 Å, $\alpha = \beta = = 90°$, $\gamma = 92.114°$, V = 611.10 Å^3

References

1. Hou, Z.; Zhang, X.; Ao, H.; Liu, M.; Zhu, Y.; Qian, Y., Passivation effect for current collectors enables high-voltage aqueous sodium ion batteries. *Materials Today Energy* **2019,** *14*, 100337.

2. Min, B. S.; Jang, W. J.; Jung, K.-N.; Kim, K. B.; Yang, J. H., NaTi2(PO4)3 nanoparticles embedded in double carbon networks as a negative electrode for an aqueous sodium-polyiodide flow battery. *Electrochimica Acta* **2020,** *361*, 137075.
3. Gu, Y.; Xiao, F.; Xu, K.; Pan, X.; Li, J.; Xu, C.; Zhou, X., Outstanding electrochemical performance of sodium vanadium phosphate cathode co-modified by carbon-coating and titanium-doping for Na-ion batteries. *Ceramics International* **2019,** *45* (9), 12570-12574.
4. Tao, H.; Zhou, M.; Wang, K.; Cheng, S.; Jiang, K., Glycol Derived Carbon- TiO2 as Low Cost and High Performance Anode Material for Sodium-Ion Batteries. *Scientific Reports* **2017,** *7* (1), 43895.
5. Hung, T.-F.; Lan, W.-H.; Yeh, Y.-W.; Chang, W.-S.; Yang, C.-C.; Lin, J.-C., Hydrothermal Synthesis of Sodium Titanium Phosphate Nanoparticles as Efficient Anode Materials for Aqueous Sodium-Ion Batteries. *ACS Sustainable Chemistry & Engineering* **2016,** *4* (12), 7074-7079.
6. Chandra, M.; Khan, T. S.; Shukla, R.; Ahamad, S.; Gupta, A.; Basu, S.; Haider, M. A.; Dhaka, R. S., Diffusion coefficient and electrochemical performance of NaVO3 anode in Li/Na batteries. *Electrochimica Acta* **2020,** *331*, 135293.
7. Zhang, S. S.; Xu, K.; Jow, T. R., *Electrochimica Acta* **2006,** *51* (8), 1636-1640.
8. Nakamoto, K.; Sakamoto, R.; Ito, M.; Kitajou, A.; Okada, S., Effect of Concentrated Electrolyte on Aqueous Sodium-ion Battery with Sodium Manganese Hexacyanoferrate Cathode. *Electrochemistry* **2017,** *85* (4), 179-185.
9. Nakamoto, K.; Sakamoto, R.; Sawada, Y.; Zhao, L.; Ito, M.; Okada, S., Aqueous Alkali Metal-Ion Battery with Hexacyanometallate Electrodes and Concentrated Electrolyte. *ECS Meeting Abstracts* **2019,** *MA2019-03* (2), 96.
10. Jiang, L.; Liu, L.; Yue, J.; Zhang, Q.; Zhou, A.; Borodin, O.; Suo, L.; Li, H.; Chen, L.; Xu, K.; Hu, Y.-S., High-Voltage Aqueous Na-Ion Battery Enabled by Inert-Cation-Assisted Water-in-Salt Electrolyte. *Advanced Materials* **2020,** *32* (2), 1904427.
11. Tang, Y.; Li, W.; Feng, P.; Zhou, M.; Wang, K.; Wang, Y.; Zaghib, K.; Jiang, K., High-Performance Manganese Hexacyanoferrate with Cubic Structure as Superior Cathode Material for Sodium-Ion Batteries. *Advanced Functional Materials* **2020,** *30* (10), 1908754.
12. Deshmukh, J.; Zhang, L.; Zhang, N.; Dutta, A.; Ye, Z.; Hijazi, H.; Yue, M.; Tulloch, M.; Johnson, M.; Metzger, M., Improving Sodium Manganese Hexacyanoferrate with Optimized Synthesis Conditions, Effective Drying, and Small Amounts of Nickel. *Journal of The Electrochemical Society* **2025,** *172* (2), 020516.
13. Gebert, F.; Cortie, D. L.; Bouwer, J. C.; Wang, W.; Yan, Z.; Dou, S.-X.; Chou, S.-L., Epitaxial Nickel Ferrocyanide Stabilizes Jahn–Teller Distortions of Manganese Ferrocyanide for Sodium-Ion Batteries. *Angewandte Chemie International Edition* **2021,** *60* (34), 18519-18526.
14. Lee, E.; Persson, K. A., Structural and Chemical Evolution of the Layered Li-Excess LiMnO3 as a Function of Li Content from First-Principles Calculations. *Advanced Energy Materials* **2014,** *4* (15), 1400498.
15. Mortazavi, M.; Wang, C.; Deng, J.; Shenoy, V. B.; Medhekar, N. V., Ab initio characterization of layered MoS2 as anode for sodium-ion batteries. *Journal of Power Sources* **2014,** *268*, 279-286.
16. (a) Henkelman, G.; Arnaldsson, A.; Jónsson, H., A fast and robust algorithm for Bader decomposition of charge density. *Computational Materials Science* **2006,** *36* (3), 354-360; (b) Han, J.; Lin, Y.; Yang, Y.; Zuo, D.; Wang, C.; Liu, X., Dominant role of M element on the stability and properties of Prussian blue analogues NaxMFe(CN)6 (M = 3d transition metal) as cathode material for the sodium-ion batteries. *Journal of Alloys and Compounds* **2021,** *870*, 159533.
17. Ma, Y.; Yang, H.; Guo, J.; Sathe, C.; Agui, A.; Nordgren, J., Structural and electronic properties of low dielectric constant fluorinated amorphous carbon films. *Applied Physics Letters* **1998,** *72* (25), 3353-3355.